Journal of Zhejiang University-SCIENCE A (Applied Physics & Engineering) 2024 25(9):749-762
www.jzus.zju.edu.cn; www.springer.com/journal/11582
E-mail: jzus_a@zju.edu.cn

Research Article

https://doi.org/10.1631/jzus.A2300372

Chemical oxygen demand oxidation via sustained-release persulfate balls: a rate-compatibility study of flow velocity, releasing, and oxidation

Bate BATE[1], Danting ZHANG[2]✉, Jianshe YE[3], Min XIA[4], Yixin YANG[1], Shuai ZHANG[1]

[1]*Institute of Geotechnical Engineering, Zhejiang University, Hangzhou 310058, China*
[2]*Shanghai Envirunion Eco-technology Co., Ltd., Shanghai 201106, China*
[3]*China Railway Eryuan Engineering Group East China Survey and Design Co., Ltd., Hangzhou 310043, China*
[4]*The Architectural Design & Research Institute of Zhejiang University Co., Ltd., Hangzhou 310027, China*

Abstract: Identification of chemical oxygen demand (COD) in municipal solid waste (MSW) landfill leachates is a challenging problem. This paper investigated the feasibility of using sodium persulfate (PS), a strong oxidant, as a permeable reactive barrier (PRB) filling material. Firstly, sustained-release persulfate balls were manufactured to adjust the release rate of persulfate, the oxidation agent. In addition, Fe(II)-loaded activated carbon (Fe-AC) was used to help with an even distribution of Fe(II) in the porous medium (PRB in this case). Then, the oxidation efficiency and kinetic rate of COD removal by the sustained-release balls were subjected to batch tests. A mass ratio of 1:1.4:0.24:0.7 for PS:cement:sand:water was the most efficient for COD removal (95%). The breakthrough curve for a 5 mm sustained-release ball revealed that the retardation factor was 1.27 and that the hydrodynamic dispersion coefficient was 15.6 cm^2/d. The corresponding half-life of COD oxidation was 0.43 d, which was comparable with the half-life of PS release from sustained-release balls (0.56 d). The sustained-release persulfate balls were shown to be an economical material with a simple recipe and production method when catalyzed by Fe-AC. Compared with cutting-edge methods, sustained-release balls used in PRBs offer significant advantages in terms of both effectiveness and economy for the preparation of sustained-release and catalytic materials. These results verified the feasibility of using sustained-release persulfate balls as a PRB material for COD removal.

Key words: Chemical oxygen demand (COD); Sodium persulfate (PS); Sustained-release balls; Permeable reactive barrier (PRB); Fe(II)-loaded activated carbon (Fe-AC)

1 Introduction

Municipal solid waste (MSW) landfills are the most common type of sanitary landfills, both inside and outside downtown areas, and can pollute soil and groundwater with biodegradation products (Dumont et al., 2017). Among these are organic compounds, designated as chemical oxygen demand (COD), consisting primarily of humic acids and fulvic acids, which are difficult to remove by degradation or oxidization (Ye et al., 2019). The concentration of COD can be as high as 10000 mg/L in the leachate, yet it is often lowered to less than 500 mg/L near MSW piles, a concentration range that can be cleaned by a permeable reactive barrier (PRB) (Han et al., 2016).

Compared with ammonium persulfate and potassium persulfate, sodium persulfate (PS) is stable and safe in terms of its melting point, relative density, water solubility, pH, and half-lethal dose of acute poisoning. PS can be easily dissociated in water to release persulfate anions. It is also stable and requires certain conditions, such as heat, ultraviolet (UV) light, or the presence of transition metals (Tsitonaki et al., 2010; Li, 2018), to generate sulfate radical anions. Given their high oxidation potential, these anions can oxidize most organic contaminants via three types of chemical reactions, namely, the detachment of hydrogen (Eq. (1)) for saturated organic compounds (alkanes,

✉ Danting ZHANG, delphinezhangdanting@gmail.com
Bate BATE, https://orcid.org/0000-0002-8692-8402
Danting ZHANG, https://orcid.org/0009-0004-0360-8932

Received July 31, 2023; Revision accepted Dec. 20, 2023;
Crosschecked Aug. 14, 2024

ethers, alcohols, and esters, represented by R); one-electron oxidation (Eq. (2)) for organic contaminants with benzene rings (benzodiazepines, aromatics); the addition of multiple bonds (Eq. (3)) for unsaturated olefin and alkyne organic compounds (Neta et al., 1977; Clifton and Huie, 1989; Padmaja et al., 1993; Khursan et al., 2006).

$$SO_4^{-}\cdot + RH \rightarrow HSO_4^{-}R, \quad (1)$$

$$SO_4^{-}\cdot + H_2C=CHR \rightarrow OSO_2OCH_2-C\cdot HR, \quad (2)$$

$$SO_4^{-}\cdot + R-Ar \rightarrow [R-Ar-CHR \rightarrow SO_4^{-}\cdot] \rightarrow SO_4^{2-} + R-Ar\cdot. \quad (3)$$

Certain metal ions, such as iron, can catalyze PS and generate higher oxidation state sulfate radicals for oxidizing organic compounds. When used as an activator for PS in PRB, metal ions should be carried by porous media. Carbon-based materials, such as activated carbon (AC) fibers, multi-wall carbon nanotubes, AC, coal-based carbon membranes, and biochar, are commonly used as carriers in the PRB because of their high chemical and physical activities, lack of secondary pollution, good biocompatibility, good acid and alkali resistance, and controllability (Table 1) (Feng et al., 2015; Li ZJ et al., 2016; Zhang et al., 2016; Hussain et al., 2017; Wang, 2017; Song et al., 2018; Dong B et al., 2019; Lee et al., 2020; Ma et al., 2023a, 2023b). Compared with AC, graphene and multi-wall carbon nanotubes are less commonly used because of their high cost. AC is inexpensive and has a well-developed pore structure, high specific surface area, and surface chemical groups (i.e., hydroxyl and carboxyl groups). It is environmentally friendly, strongly adsorptive to ions, and easy to modify. Therefore, AC has been widely used as a catalyzing agent carrier and high-capacity absorbent (Veerakumar et al., 2016; Kamaraj et al., 2020; Singh et al., 2023). Iron, an economical and abundant natural material, is often used as a cost-effective and environmentally friendly option for modifying AC. It readily attaches to PS-loaded AC and serves not only as an absorbent material but also as a heterogeneous catalyst (Li et al., 2016b; Lee et al., 2020; Zhao et al., 2021, 2023). Divalent iron fixation on granular AC has been widely used in PRB (Goyal et al., 2023). Zhao et al. (2021) reported that Fe(II)-loaded activated carbon (Fe-AC), as a catalyst material for the oxidant reaction, exhibited stability with low leakage of iron cations. Although iron-loaded AC can catalyze PS to oxidize organic compounds effectively (Li J et al., 2016; Kalaruban et al., 2019), to date, its ability to oxidize organic compounds (COD) from MSW pile leachates has not been reported.

Following a comparison of methods for preparing sustained-release materials, such as coating, freeze–thaw, sol–gel, and oil–phase separation, and mixing with binders, a cost-effective, time-efficient, and user-friendly approach was chosen (Kang et al., 2004; Lee and Schwartz, 2007; Liang et al., 2011; Lin et al., 2012; Rauscher et al., 2012; Chen et al., 2013; Lee and Gupta, 2014; Sakulthaew and Chokejaroenrat, 2016; Yang et al., 2016; Omoike and Harmon, 2019; Wang et al., 2023). As reported by Wang et al. (2023), the release of PS from pellets fits a second-order kinetics equation. However, the reaction is affected by the large area of pores and cracks. This method involves mixing cement, sand, and water with oxidizing agents, such as PS, to produce sustained-release PS balls with a mass ratio of 1:1.4:0.24:0.7 for PS:cement:sand:water. Sustained-release balls with a certain ratio

Table 1 Catalyst types of persulfate

Catalyst	Contamination	Reference
N-doped coal-based carbon membrane	Bisphenol A (BPA)	Ma et al. (2023b)
Fe_3O_4/multi-walled carbon nanotubes	Flumequine	Feng et al. (2015)
Fe_2O_3 nanoparticle/oxidize carbon nanotube membrane	Tetracycline (TCE)	Ma et al. (2023a)
$CuFe_2O_4$/AC	Coking wastewater	Song et al. (2018)
$CuFe_2O_4$/multi-walled carbon nanotubes	Diethyl phthalate (DEP)	Zhang et al. (2016)
nZVI/rice husk biochar	Phthalate	Dong CD et al. (2019)
nZVI/biochar	Nonyl phenol	Hussain et al. (2017)
Fe^{2+}/AC	Perfluorooctanoic acid	Lee et al. (2020)
Fe^{2+}/AC	Landfill leachate (COD)	Li et al. (2016b)
Iron-based sludge biochar	Organic wastewater	Wang (2017)

nZVI: nanoscale zero-valent iron

of PS ensure the continuous release of the oxidizing agent ($S_2O_8^{2-}$) (Liang et al., 2011). The price of sustained-release persulfate balls was calculated to be 3.3 CNY/kg.

In PRB engineering, the sustained release of PS is needed. However, PS has a short half-life and cannot be used directly as a PRB filling material (Lee et al., 2020; Zhao et al., 2021, 2023). The selection of filling materials for PRBs should consider the potential formation of precipitates, as they can lead to barrier clogging, reducing both permeability and overall effectiveness (Budania and Dangayach, 2023). In addition, the temporospatial heterogeneity of persulfate oxidation due to preferential flow in the PRB can generate pore-blocking precipitates and bypass flow, which makes contaminants in low-permeability zones difficult to degrade (Ross et al., 2005). To address the above problems, processed sustained-release balls of PS were manufactured to control the release rate of PS and increase its lifetime. At present, no quantitative study is available on the release time of sustained-release PS balls or their compatibility with the oxidation time for COD removal.

This study aimed to explore the feasibility of implementing PS sustained-release balls in a PRB and to obtain the matched chemical kinetics for the sustained release of PS and the COD oxidation reaction by optimizing the ball size.

2 Materials and experimental methods

2.1 Materials

The particle size of the AC used in this study ranged from 1 to 2 mm (Shanghai Xinhui Activated Carbon Co., Ltd., China). The cement used was PI 42.5 Portland cement (China General Academy of Building Materials Science Research Co., Ltd.). The analytical reagents potassium hydrogen phthalate ($C_8H_5KO_4$), PS ($Na_2S_2O_8$), iron vitriol ($FeSO_4·7H_2O$), potassium dichromate ($K_2Cr_2O_7$), sulfuric acid (H_2SO_4), silver sulfate (Ag_2SO_4), mercury sulfate ($HgSO_4$), potassium iodide (KI), and sodium bicarbonate ($NaHCO_3$) were used in this study. Contaminated leachate samples were collected from Hangzhou Tianziling Landfill, China and were stored in a freezer before testing. The COD concentration of the leachate was determined to be 778 mg/L.

Fe-AC with grain sizes of 1 to 2 mm was produced as follows: AC was soaked in 1% sulfuric acid overnight, rinsed with deionized water, and oven-dried for 24 h at 105 ℃. Ten grams of oven-dried AC were mixed with 50 mL of 0.1 mol/L iron vitriol solution in a thermostatic oscillator for 1 h to load divalent iron on the AC surface. The resulting Fe-AC was oven-dried for 2 h at 65 ℃ and then calcined in a tubular furnace at 550 ℃ under nitrogen to oxidize the divalent iron (Li, 2016). The Fe-AC was stored in a vacuum dryer before use.

Sustained-release PS balls with grain sizes ranging from 5 to 20 mm were manufactured by the College of Civil Engineering and Architecture, Zhejiang University, China. Ottawa sand with a diameter range of 20–30 meshes and cement were manufactured by China General Academy of Building Materials Science Research Co., Ltd. PS, cement, sand, and water were prepared at the ratios mentioned above. In a 500 mL beaker, PS, cement, and sand were added, followed by the addition of water. The components were continuously mixed for 15–20 min. The resulting paste liquid was poured into molds with diameters ranging from 5 to 20 mm and air-dried for 1 d at room temperature (25 ℃) to fix the shape (Liang et al., 2011).

2.2 Experimental methods

2.2.1 Microscopic characterization

Nitrogen adsorption tests on unmodified AC and Fe-AC samples were performed via a fully automatic specific surface and micropore size analyzer to measure the specific surface area, total pore volume, and pore distribution. For the pore throat structure, a Micrometrics AutoPore IV 9500 mercury intrusion porosimeter (MIP) was used at a pressure of 206.844 MPa in the test.

Unmodified and Fe-AC samples were tested for topography and elemental analysis by scanning electron microscopy (SEM) and electron energy dispersive spectroscopy (EDS).

Fe-AC or unloaded AC samples were taken for mineral composition and functional group tests via X-ray diffraction (XRD) and Fourier transform infrared (FTIR) spectroscopy methods. XRD was performed via an Advance D8A25 powder X-ray diffractometer (Bruker, Germany), and the data were analyzed via MDI Jade 6 software (v. 6.5.26; Material Data, Inc., CA, USA) and a Nicolet iS50FT-IR Instrument

(Thermo Scientific, USA) for FTIR; 32 scans with a resolution from 400 cm^{-1} to 4000 cm^{-1} were collected with a KBr of 4 cm^{-1} (scanning resolution).

2.2.2 Chemical concentrations

To determine the COD removal efficiency of PS oxidation, batch tests were performed according to the following steps: (1) 100 mL of contaminated solution was diluted twice, and 0.278 g of iron vitriol or PS (0.119 g, 0.238 g, 0.476 g, or 1.19 g) was added to a 250 mL conical flask. (2) The volume of 100 mL of contaminated solution was diluted twice, and PS (0 g, 0.119 g, 0.238 g) and 1 g of unloaded AC samples were placed in a 250 mL conical flask. (3) A total of 100 mL of contaminated solution was diluted twice, and PS (0.500 g, 0.238 g, and 0.476 g) and 1 g of Fe-AC were added to a 250 mL conical flask. The conical flasks were placed in a thermostatic oscillator at a temperature of 20 ℃ and a 150 r/min rotation speed, and then, 1 mL of sample was taken at time points of 20, 40, 60, 80, 100, and 120 min for the COD concentration tests. The sample collection method followed the aquarium leaching test according to EA NEN 7375 (CEN, 2004), which was carried out to obtain the release rate of cement sustained-release balls (Kosson et al., 1996; Chen et al., 2013). In the leaching experiment, sustained-release PS balls with particle sizes ranging from 5 to 20 mm with 100 mL of deionized water were placed in 250 mL conical flasks, the leaching solution was replaced, and samples were taken according to a timetable at 0.25, 1, 2.25, 4, 9, 16, 32, and 64 d. The concentration of sodium ions was obtained via an S23A visible light spectrophotometer (Shanghai Lengguang Technology Co., Ltd., China) at 352 nm to estimate the cumulative release volume and release rate of PS according to Eq. (4).

$$q=\frac{C_1V}{M}, \tag{4}$$

where q is the cumulative release amount (mg/g); C_1 is the concentration of sodium ions; V is the volume of deionized water; M is the mass of the sustained-release PS balls.

To obtain the release rate of the sustained-release PS balls, a batch test was carried out as follows: 100 mL of the twice-diluted contaminated solution was placed in 250 mL conical flasks, together with 1 g of Fe-AC and two or four pebbles of sustained-release PS balls, which contained either 1 or 2 mmol of PS. The flasks were placed in a thermostatic oscillator with a 150 r/min rotation speed at 20 ℃. A 1 mL sample was obtained for COD concentration measurement at time steps of 20, 40, 60, 80, and 100 min, as well as at 2, 4, 6, 24, and 48 h.

Inductively coupled plasma–mass spectrometry (ICP–MS) (ICAPRQICPMS, Thermo Fisher Scientific, USA) was used for the iron concentration test.

Rapid-resolution spectrophotometry tests were performed to measure the COD concentration. The volume of 1 mL of 0.24 mg/L Ag_2SO_4 and 0.5 mol/L 1/6$K_2Cr_2O_7$ (Ag_2SO_4:$K_2Cr_2O_7$=1:2 (mole ratio)) solution, with 4 mL of 10 g/L sulfuric acid–silver sulfate solution, was placed in a Hash digestion tube, shaken well, added to 2 mL of sample, and digested for 15 min at 165 ℃ in the digester. The absorbance was measured after cooling at 440 nm for concentrations ranging from 15 to 250 mg/L and at 600 nm for concentrations ranging from 100 to 1000 mg/L.

The persulfate concentration was determined spectrophotometrically via the iodometry method. First, a 0.2 mmol/L PS stock solution was prepared. Then, 0.00, 2.00, 4.00, 6.00, 10.00, and 12.00 mL stock solutions were separately pipetted into 50 mL test tubes and diluted with deionized water. Third, 0.2 g of sodium hydrogen carbonate and 4 g of potassium iodide were added, and the mixture was diluted to 50 mL with deionized water and shaken for the full-color reaction. The relationship between the absorbance at 352 nm and the persulfate concentration was highly linear, with R^2=0.991, as illustrated in Fig. 1 (Guo, 2013). The equation (y=0.0475x−0.0038) can be applied to calculate the PS residue in the kinetic experiment of the COD oxidation reaction, enabling the determination of COD concentrations.

2.2.3 Preparation method for sustained-release PS balls

The mass ratio of PS:sand:cement:water was set to 1:0.24:1.4:0.7, which was the ratio used by Liang et al. (2011). The sand content was the dominant factor for the sustained release of PS at sand:cement ratios greater than 1, as opposed to the cement-dominant ratio, i.e., a sand:cement ratio less than 1.

The breakthrough test was performed in a plexiglass column (Fig. 2) with a length of 50 cm and a diameter of 5 cm. The filler materials, from bottom to

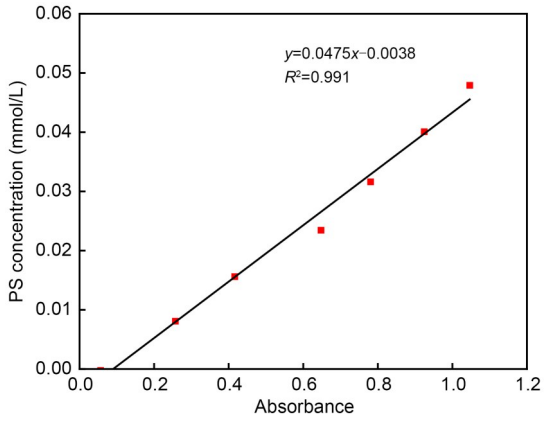

Fig. 1 Relationship between the PS concentration and absorbance

top, were Ottawa sand with the filling thickness of 15 cm, sustained-release PS balls (5 cm; approximately 380 pebbles), Ottawa sand (10 cm), Fe-AC (5 cm), Ottawa sand (5 cm), AC (5 cm), and Ottawa sand (5 cm) (Table 2). There were three sample collection holes on the sidewall at distances of 20, 35, and 50 cm from the column base. The inflow solution, with a diluted COD concentration of 200 mg/L and a pH of 7.1, was peristaltically pumped from the column base at a flow rate of 0.3 mL/min. Effluent samples were collected at specified intervals and stored in a dark environment for COD concentration measurement. The ambient temperature was 15 °C.

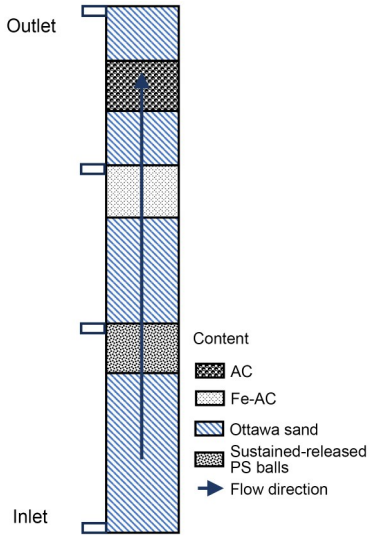

Fig. 2 Break-through column test setup

Table 2 Properties of the PRB filler materials from bottom to top as shown in Fig. 2

Filling materials (from bottom to top)	Filling thickness (cm)	Filling mass (g)
Ottawa sand	15	493
Sustained-release PS balls	5	122
Ottawa sand	10	388
Fe-AC	5	62
Ottawa sand	5	185
AC	5	61
Ottawa sand	5	181

3 Results

3.1 Microscopic characteristics

Compared with that of unloaded AC, the specific surface area of Fe-AC decreased by approximately 24% (from 1143.56 to 867.37 m^2/g). A significant decrease in microporous pore volume (Fig. 3a) was

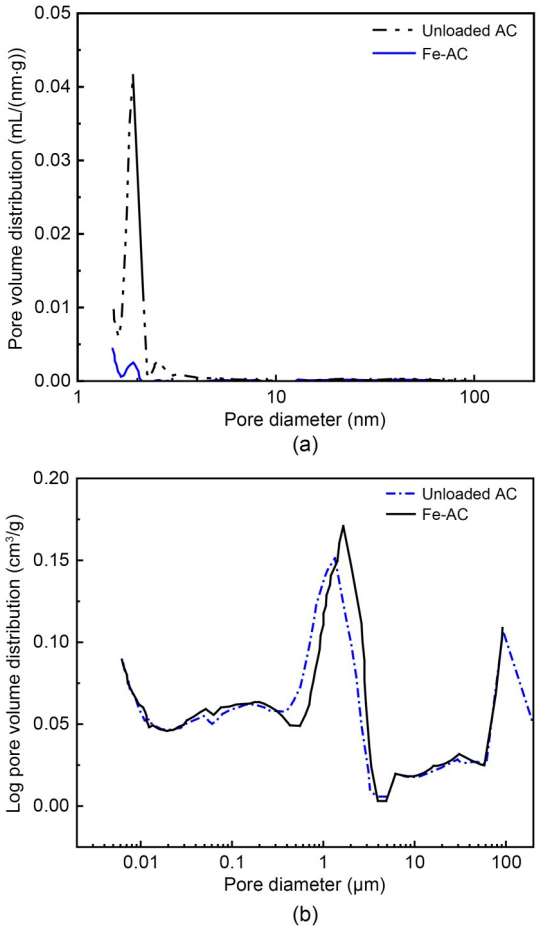

Fig. 3 Pore distributions of AC before and after iron loading via the Barret-Joyner-Halenda (BJH) (a) and mercury intrusion porosimetry (MIP) (b) methods

also observed after Fe(II) loading, probably because the crystals of Fe(II) occupied and clogged the micropores of AC (Kalaruban et al., 2019). This is supported by the decrease in the micropore radius from 1.91 nm to 1.90 nm according to the BET (Brunauer-Emmet-Teller) results and the decrease in diameter from 1.61 μm to 1.31 μm according to the mercury intrusion porosimetry (MIP) results (Fig. 3).

According to the SEM and EDS results of the Fe(II)-loaded or unloaded AC, the surface of the AC contained large amounts of small openings (Fig. 4a). The surface of the Fe-AC contained iron aggregates (Fig. 4b). PS grains with ball diameters between 170 and 200 μm were uniformly distributed in the sustained-release balls (Fig. 5). EDS of the SEM images (Fig. 6) revealed that the primary elements of the sustained-release balls were Ca and Si, which is consistent with the chemical compositions of the cement (CaO and SiO_2) and the PS inserted (Na and S).

According to the XRD results (Fig. 7), the unloaded AC primarily consisted of carbon, whereas after loading the ferro-compounds, new minerals, mainly ferric oxide (Fe_2O_3) and ferric oxide (Fe_3O_4), were identified via MDI Jade 6 software.

From the FTIR results (Fig. 8), the characteristic peaks of AC at 3431 cm^{-1}, 1560 cm^{-1}, 1384 cm^{-1}, and 1109 cm^{-1} were attributed to O–H stretching vibrations (Abdullah et al., 2018; Zhang et al., 2018), C=C bending vibrations (Barroso-Bogeat et al., 2019), CH_3 vibrations (Das et al., 2008), and C–O stretching

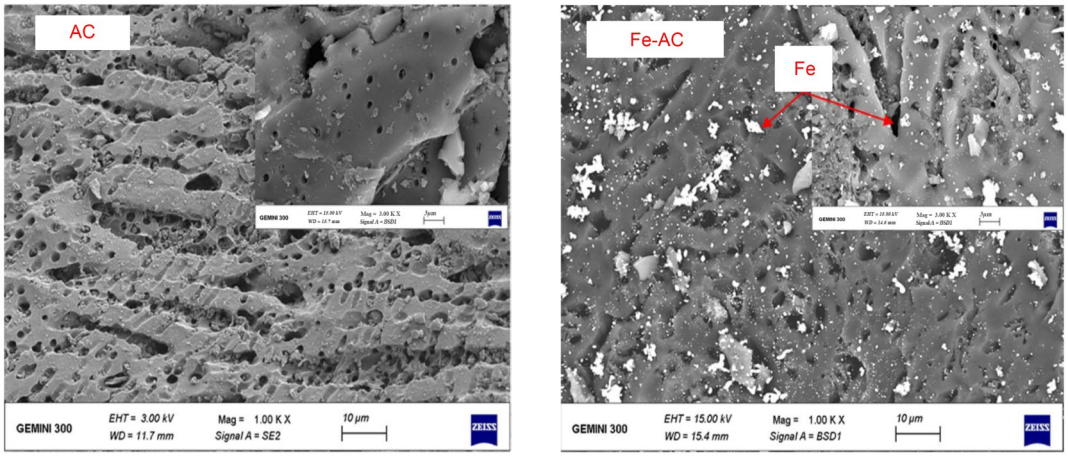

(a) (b)

Fig. 4 SEM images of AC before (a) and after (b) Fe(II) loading

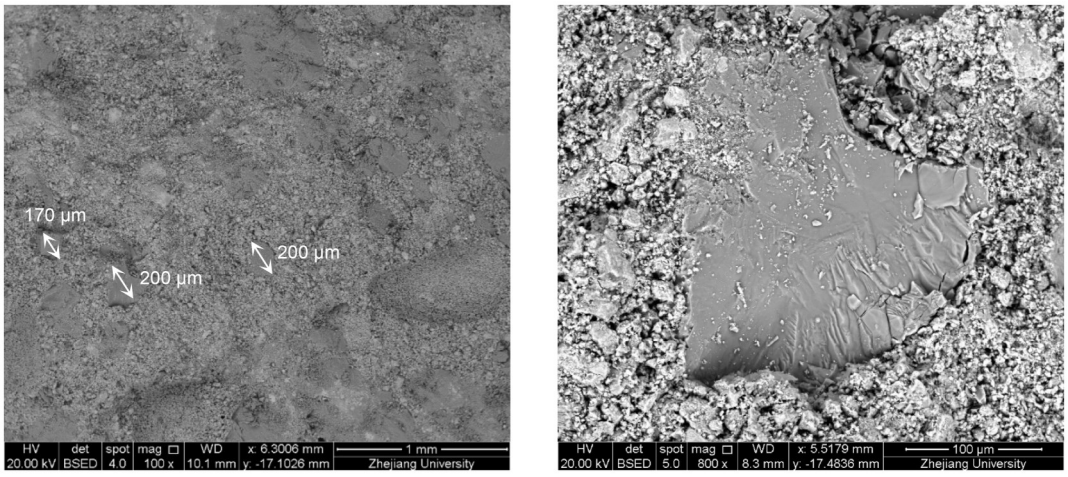

(a) (b)

Fig. 5 SEM images of sustained-release PS balls with magnification factor in 1 mm (a) and 100 μm (b)

vibrations (Cheng et al., 2016; Zhang et al., 2018), respectively. The Fe–O stretching vibration appeared with a band at 700–500 cm^{-1} (Krishnan and Haridas, 2008), and the Fe–O–H stretching vibration appeared with a band at 700–500 cm^{-1} (Mehrabi et al., 2015). The characteristic peaks of Fe-AC were changed from 3431 cm^{-1} to 3434 cm^{-1}, from 1560 cm^{-1} to 1572 cm^{-1}, and from 1109 cm^{-1} to 1120 cm^{-1}, suggesting that the intensity of Fe-AC was greater than that of unloaded AC because of the accumulation of iron contained in those functional groups. This indicates that iron was effectively loaded on the surface of the AC (Mehrabi et al., 2015).

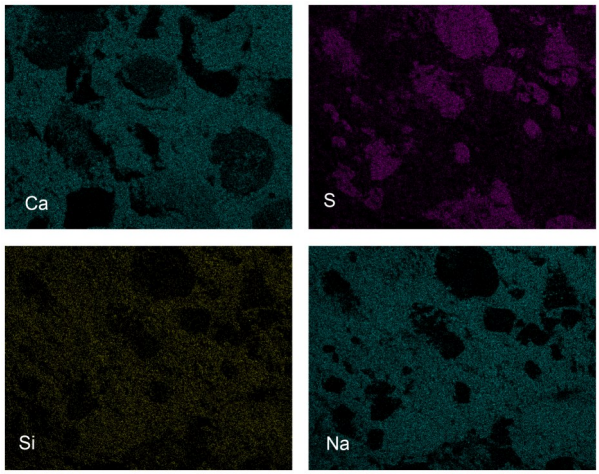

Fig. 6 EDS results of sustained-release PS balls. References to color refer to the online version of this figure

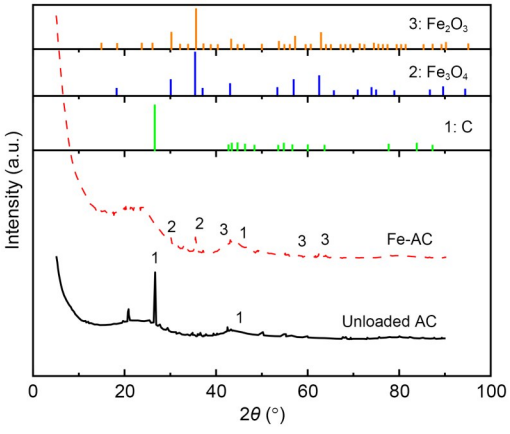

Fig. 7 XRD patterns of AC before and after Fe(II) loading

Based on the above results, it is postulated that the unique structure of Fe-AC enhances its chemical activity based on three mechanisms: (1) A large specific surface area and micropores increase the number of reaction sites for the absorbance of contaminants in the catalytic reaction. (2) The carbon of Fe-AC has a high sp2 hybrid carbon ratio, which is more conducive to the radio activation of PS because of the high defect density (Tian et al., 2018). (3) Increases in the electronic conductivity and electronic transfer capability enable the graphitization of the Fe-AC, as shown by the XRD results (Fig. 7), where a 43.3° diffraction peak emerged (2θ), which is a typical characteristic of graphitization (Gong et al., 2017). (4) Fe-AC reduces the number of local functional groups on the carbon surface and improves interfacial electron transfer (Yao et al., 2016). (5) Carbon coatings can prevent iron ions from rapidly corroding (Lee et al., 2020).

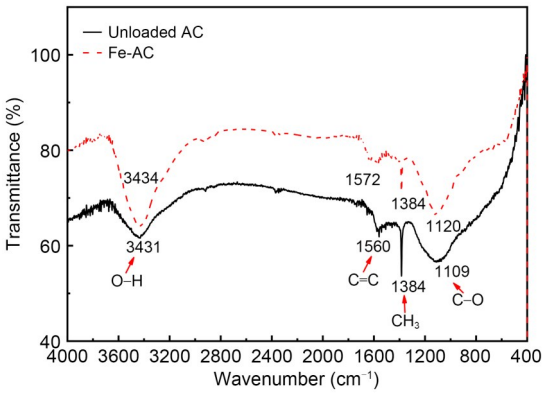

Fig. 8 FTIR spectra of AC before and after Fe(II) loading

3.2 Kinetics of the COD oxidation reaction

PS can be misidentified as the result of COD in rapid-resolution spectrophotometry, which overestimates the actual COD. The chemical reaction equation involved is as follows (Zeng et al., 2017):

$$Cr_2O_7^{2-}+3S_2O_8^{2-}+2H^+\rightarrow 2Cr^{3+}+6SO_4^{2-}+H_2O+3O_2. \quad (5)$$

Based on Eq. (5), the relationship between PS and the identified COD concentration, i.e., 1 g/L PS equals 66.88 mg/L COD, was calibrated (Fig. 9).

The actual COD concentration was subsequently obtained by subtracting the residue of PS in the sample from the measured COD concentration (Wang et al., 2014; Yang, 2016). When the first-order kinetic reaction assumption is applied to COD removal by Fe-AC-catalyzed PS, the fitted constant of the reaction rate K is 0.83 h^{-1} and the half-life period $t_{0.5}$ is 0.83 h.

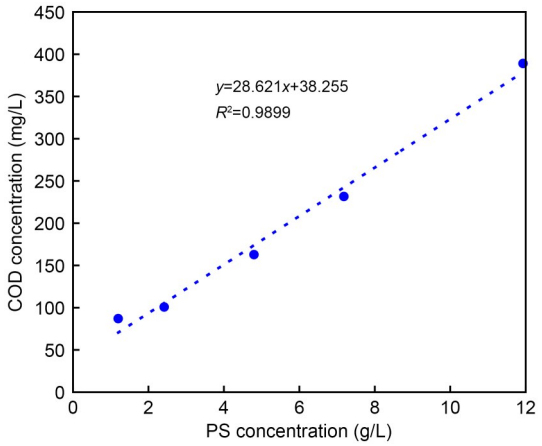

Fig. 9 Relationship between PS and COD identified by rapid resolution spectrophotometry

Applying the pseudo-first-order kinetics reaction assumption to COD removal by four pebbles of sustained-release PS balls catalyzed with Fe-AC yielded a fitted constant of the reaction rate (K) of 0.15 h^{-1} and a half-life period ($t_{0.5}$) of 4.62 h, where C denotes the concentration of COD (mg/L) and C_0 denotes the initial concentration of COD (mg/L) (Fig. 10).

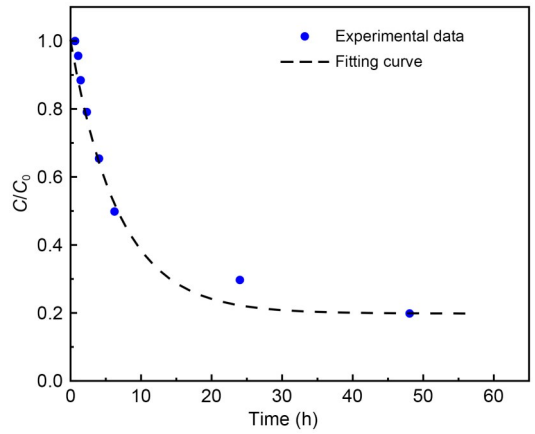

Fig. 10 Fe-AC-PPS2 (Fe-AC and four-pebble sustained-release PS balls containing 2 mmol PS) pseudo-first-order kinetics fitting curve

3.3 COD removal efficiency

As the Fe(II):PS ratio decreased from 1:0.5 to 1:1 and 1:2, the removal rates of COD increased from 68% to 80% and 95%, respectively. By Fe(II) activation, the higher ratio of PS led to the production of more sulfate radicals, which in turn oxidized more COD in the fluid. A further increase in the PS content at a Fe(II):PS ratio of 2 led to a drastic decrease in the COD removal rate (33%). Given the high activity of sulfate radicals, their abundance in the fluid could be wrongly identified as COD (elaborated in the preceding paragraph), which could yield a low COD removal rate. On the other hand, at a high PS content (Fe(II):PS) ratio of 0.5, Fe^{2+} consumes sulfate radicals ($SO_4^{\cdot-}$), leading to a low COD removal rate (68%) (Eq. (6)). Furthermore, divalent Fe^{2+} in solution is easily oxidized by oxygen in the air. Therefore, the direct addition of Fe^{2+} into the PRB is not practical. Alternatively, the Fe-AC is stable and applicable to PRB. Its effects on COD removal will be described later.

$$SO_4^{\cdot-} + Fe^{2+} \rightarrow SO_4^{2-} + Fe^{3+}. \tag{6}$$

The COD removal rates via both AC and alone were less than 27% (Fig. 11b). AC can absorb COD, and the hydroxyl and carboxyl groups on AC can further catalyze PS to generate sulfate radicals to oxidize COD (Xu et al., 2012), which improves the COD removal rates by up to 58% with AC:PS ratios of 1.

Given 1 g of Fe-AC, the COD removal rate increased from 62% to 67% and to 90% as the PS content increased from 0.119 g to 0.238 g and then to 0.476 g. At a 90% COD removal rate, the concentrations of $S_2O_8^{2-}$ and Fe^{2+} were 4.76 g/L and 8.5 g/L, respectively, and the $S_2O_8^{2-}$:12COD ratio was 1.02 (Fig. 11c). The catalysis of PS by Fe-AC resulted in an impressive COD removal rate of up to 90% while also mitigating the disadvantage of Fe^{2+} easily oxidizing in the presence of air. From the above measurements, the fitted chemical kinetic constants can be determined: the kinetic rate constant at 0.83 h^{-1} and the half-life ($t_{0.5}$) at 0.83 h.

3.5 Release rate of sustained-release PS balls

The released cumulative PS for the four particle diameters fits well with the hyperbolic kinetics models (Fig. 12; Table 4), and the relationship between the released cumulative PS amount q (mg/g) and the time t (d) is as follows:

$$\frac{1}{q} - \frac{1}{q_{\max}} = \frac{1}{kt}. \tag{7}$$

Eq. (7) can be converted to Eqs. (8)–(10) such that

$$q = q_{\max}\left(1 - \frac{1}{1 + \dfrac{kt}{q_{\max}}}\right), \tag{8}$$

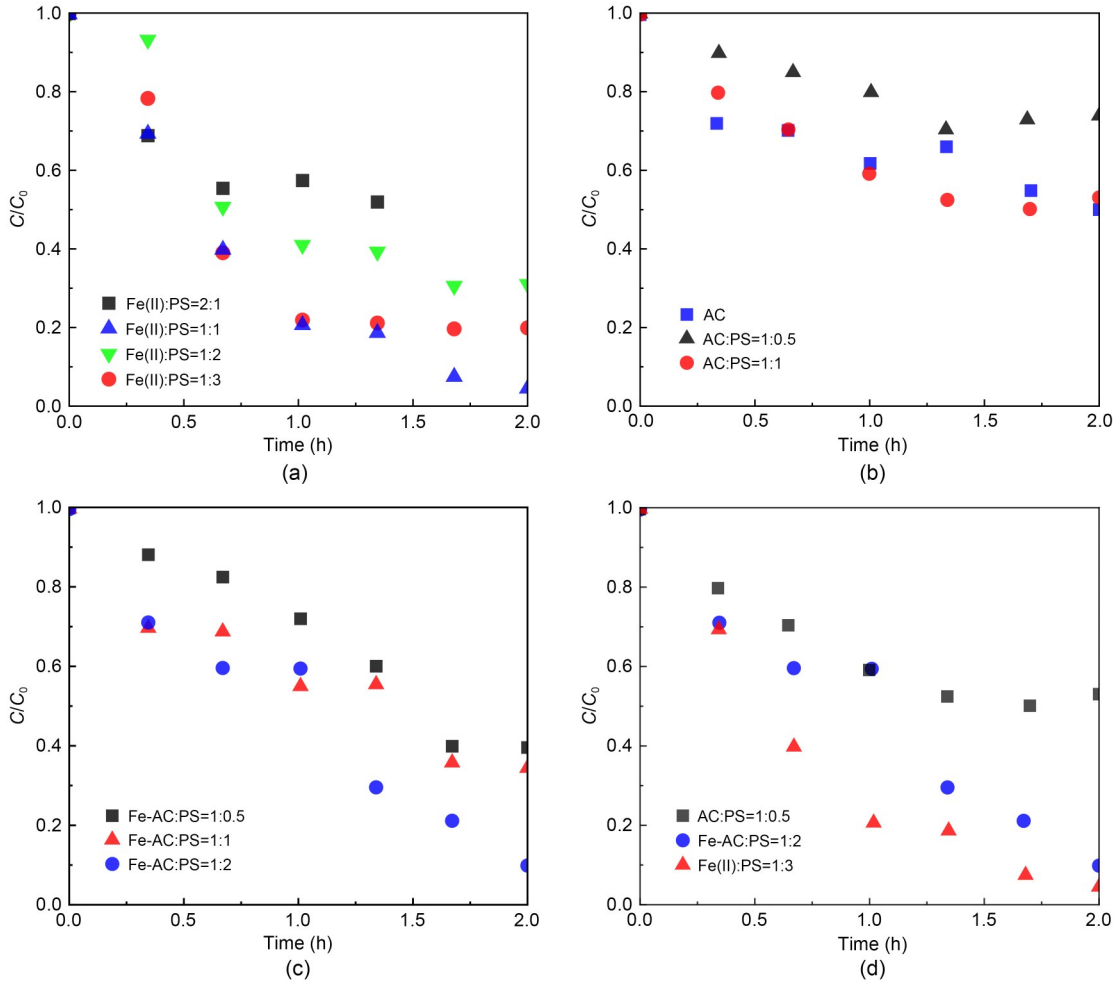

Fig. 11 Time-evolution curves of the normalized COD concentrations for Fe(II) (ferrous sulfate) and PS at different ratios (a), AC and PS at different ratios (b), Fe-AC and PS at different ratios (c), and AC and PS, Fe-AC and PS, as well as Fe(II) and PS at a certain ratio (d)

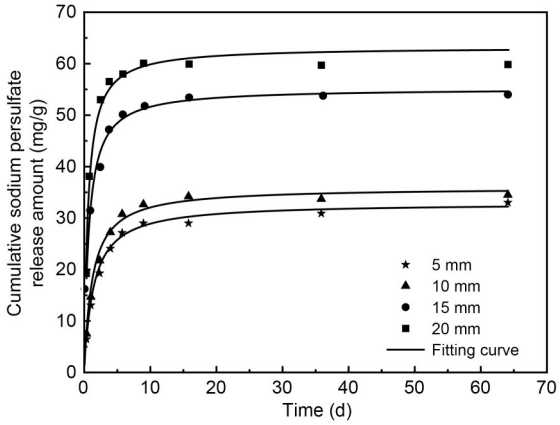

Fig. 12 PS cumulative release amount and fitting curve

$$t=\frac{q_{\max}}{k}\frac{a}{1-a}, \tag{9}$$

$$t_{0.5}=\frac{q_{\max}}{k}, \tag{10}$$

where $q_{\max}$ is the maximum released amount of the sustained-release PS balls, mg/g; k is the rate of release, mg/(g·d); $a=\frac{q}{q_{\max}}$ is the release ratio. The fitting parameters are listed in Table 3.

A linear relationship (R^2=0.945) between the ball diameter D (mm) and half-life period was observed (Fig. 13a):

$$t_{0.5}=0.060D+0.215. \tag{11}$$

The ball diameter and kinetic rate constant of PS release (k) were inversely proportional:

$$k=544.6/D,\ R^2=0.8951. \tag{12}$$

Table 3 Release rates of the sustained-release PS balls

Ball diameter (mm)	Fitting curve	Release rate (mg/(g·d))	$t_{0.5}$ (d)
5	$q_1=7098t/(63.14+112.27t)$	112.27	0.56
10	$q_2=4370t/(55.23+79.14t)$	79.14	0.70
15	$q_3=1064t/(35.92+29.60t)$	29.60	1.21
20	$q_4=778t/(32.91+23.63t)$	23.63	1.39

Table 4 Parameters of sustained-release PS balls for different sizes

Ball diameter (mm)	q_{max} (mg/g)	k (mg/(g·d))	SSE	R^2
5	63.14	112.27	14.61	0.9879
10	55.23	79.14	16.77	0.9873
15	35.92	29.60	15.82	0.9779
20	32.91	23.63	8.05	0.9872

SSE: sum of squares due to error

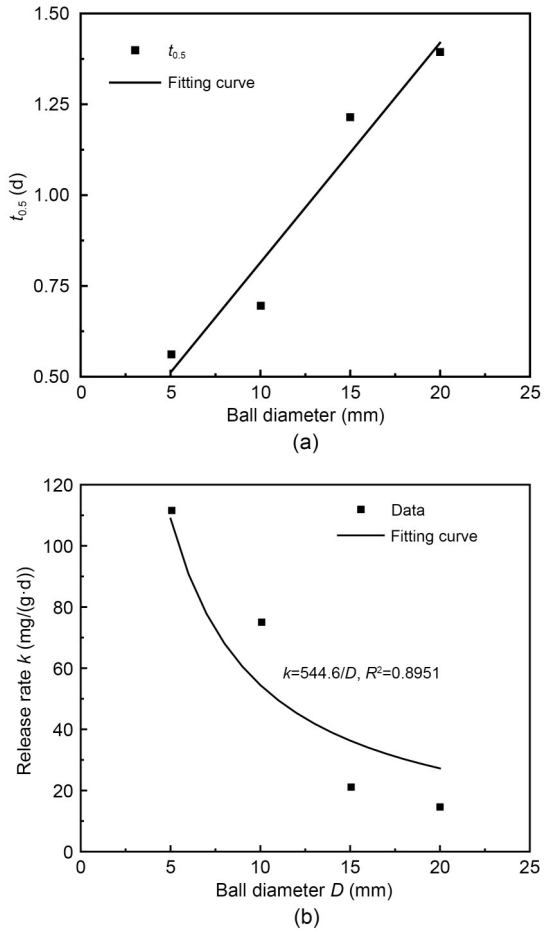

Fig. 13 Relationships and fitting curves between half-life period and ball diameter (a) and release rate and ball diameter (b)

4 Discussion

4.1 Compatibility between the PRB flow rate and the PS release rate

For an engineered PRB to work effectively, the appropriate amount of PS released should be consumed for COD oxidation. This requires that at a given time, sufficient cumulative quantity of PS (Q_{PS}) is released to oxidize the cumulative quantity of COD (Q_{COD}) in the permeation fluid. Q_{COD} is quantified as AV_0C_0t, where A denotes the PRB water cross-section (m^2), and V_0 denotes the flow rate (m/d). Q_{PS} is quantified as $\frac{A}{D^2}Mk\times10^9$, where M is the mass of the sustained-release balls (g per unit).

Given 2500 20 mm sustained-release PS balls in a PRB cross-section area, with M=8.85 g per unit, the release rate (k) is 23.63 mg/(g·d), and the released PS is 522.81A g/d, which can oxidize COD 42.7A g/d (Fig. 14). Given the COD concentration of 200 mg/L, the maximum flow rate in the PRB is 0.21 m/d.

According to the batch test, the ratio of Q_{COD}:Q_{PS} is at equilibrium, namely:

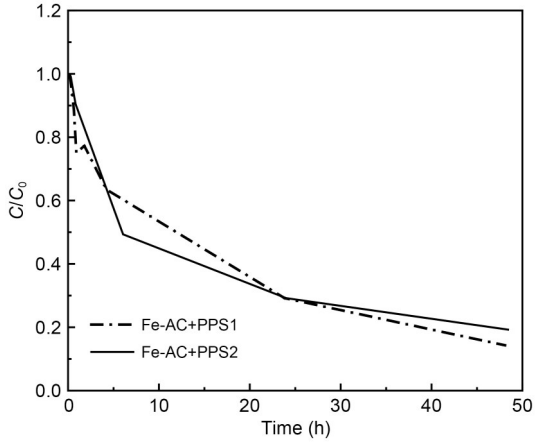

Fig. 14 Removal effect of COD with an oxidizing filler by using Fe-AC with two pebbles (PPS1) and four pebbles (PPS2) of sustained-release PS balls

$$aAV_0C_0 \leqslant \frac{A}{D^2Mk} \times 10^6. \tag{13}$$

4.2 Compatibility of the PS release rate and COD oxidation rates

To allow sufficient time for COD oxidation, the rate constant of COD consumption (oxidation) should be similar to the PS release rate. The kinetic chemical reaction results of the Fe-AC-catalyzed sustained-release PS balls oxidizing COD (Fig. 15) can be fitted (R^2=0.9452) by the first-order kinetic reaction:

$$R_{\mathrm{COD}} = K_1 \cdot \frac{\partial C_{\mathrm{COD}}}{\partial t}, \tag{14}$$

where the half-life is 0.43 d and the rate constant K_1 is 0.08 h^{-1}. The oxidation reaction half-life (0.43 d) is close to the PS release half-life of a 5 mm diameter ball (0.56 d), which satisfies the compatibility condition (Fig. 15).

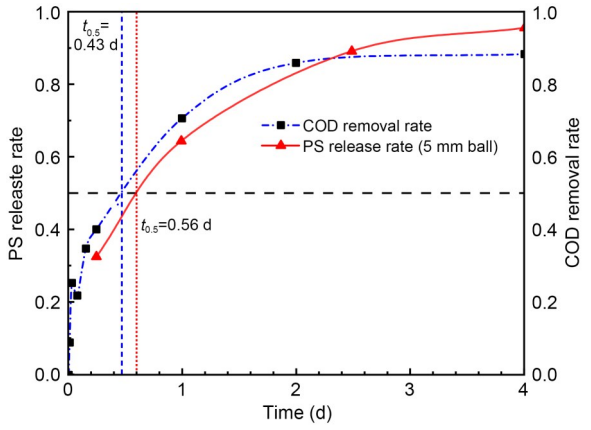

Fig. 15 Kinetic chemical reaction results of Fe-AC-catalyzed sustained-release PS balls that oxidize COD

4.3 Simulation of PRB serviceability

The COD concentration from the effluent in the column test was greater than 80% after 40 h. With the use of STANMOD-CXTFIT software, the retardation factor R_d and the hydrodynamic dispersion coefficient D_h were estimated to be 1.27 and 15.6 cm^2/d, respectively, via the following equation (Fig. 16):

$$\frac{C_f}{C_0} = \frac{1}{2}\mathrm{erfc}\left(\frac{R_dL - V_st_b}{2\sqrt{D_hR_dt_b}}\right) + \frac{1}{2}\exp\left(\frac{V_sL}{D_h}\right)\mathrm{erfc}\left(\frac{R_dL + V_st_b}{2\sqrt{D_hR_dt_b}}\right), \tag{15}$$

where C_f is the outflow concentration; L is the thickness of the seepage path; V_s is the flow rate of pore water; t_b is the breakthrough time.

Given that V_0=0.21 m/d, R_d=1.27, and L=3 m (thickness of the PRB), the service life of this PRB with a breakthrough threshold of 10% is two years, which is practical.

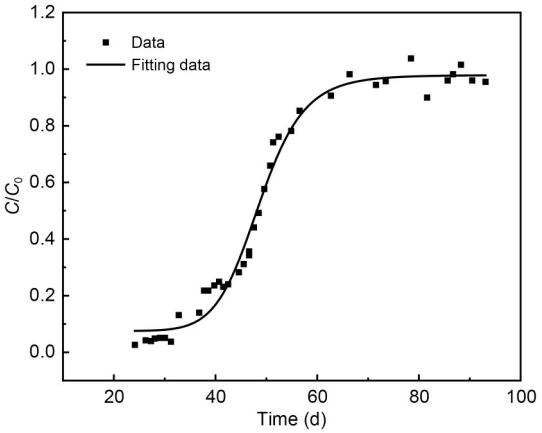

Fig. 16 Breakthrough curve of COD in a column test

5 Conclusions

The feasibility of the use of PS as a strong oxidant in a PRB was verified in terms of the COD oxidation efficiency and the rate of chemical kinetic reactions. An increase in oxidation efficiency was achieved by Fe-AC, which helps evenly distribute Fe(II), a high-efficiency oxidant, in the PRB. The test results demonstrated the feasibility of the use of PS in the PRB:

(1) The optimum dosage ratios of Fe-AC: sustained-release PS balls and PS:COD were initially 1:2 and 12.24:1, respectively, which yielded the highest COD removal rate of 95%.

(2) The release rate (k) of sustained-release PS balls was inversely proportional to the ball diameter D, namely, k=544.6/D. In addition, the COD oxidation rate ($t_{0.5}$=0.43 d) was compatible with the PS release rate of balls under 5 mm ($t_{0.5}$=0.56 d). This substantiated the compatibility of the release rate of sustained PS balls and the kinetic oxidation rate of COD.

(3) The COD removal by PS catalyzed by Fe-AC followed first-order kinetics, with a rate constant of 0.83 h^{-1} (i.e., $t_{0.5}$=0.83 h). Similarly, COD removal by four pebbles of sustained-release PS balls catalyzed by Fe-AC followed pseudo-first-order kinetics, with a

rate constant of 0.15 h^{-1} (i.e., a half-life of 4.62 h), which might be due to the pores and cracks on the balls.

(4) Compared with certain new carbon-based materials used in PRB for COD removal, the sustained-release PS balls addressed the issue of the high effectiveness of PS, which, owing to the blocking risk and fast reaction rate, might otherwise be unsuitable as a PRB filling material. Based on the kinetic parameters discussed earlier, the sustained-release PS balls, catalyzed by Fe-AC, clearly exhibited high COD removal effectiveness.

Acknowledgments

This work is supported by the Ministry of Science and Technology of China (Nos. 2019YFC1805002 and 2018YFC1802300), the National Natural Science Foundation of China (Nos. 42177118 and 51779219), the Basic Science Center Program for Multiphase Evolution in Hypergravity of the National Natural Science Foundation of China (No. 51988101), and the Overseas Expertise Introduction Center for Discipline Innovation (No. B18047), China. The authors would also like to acknowledge the MOE Key Laboratory of Soft Soils and Geoenvironmental Engineering, China.

Author contributions

Bate BATE: original idea, funding acquisition, advising, and revision. Danting ZHANG: experiments, analysis, and writing–original draft. Jianshe YE: experiments, analysis, writing–review & editing. Min XIA: project administration and data curation. Yixin YANG: writing–review & editing. Shuai ZHANG: writing–review & editing.

Conflict of interest

Bate BATE, Danting ZHANG, Jianshe YE, Min XIA, Yixin YANG, and Shuai ZHANG declare that they have no conflict of interest.

References

Abdullah B, Ilyas S, Tahir D, 2018. Nanocomposites Fe/activated carbon/PVA for microwave absorber: synthesis and characterization. *Journal of Nanomaterials*, 2018: 9823263. https://doi.org/10.1155/2018/9823263

Barroso-Bogeat A, Alexandre-Franco M, Fernández-González C, et al., 2019. Activated carbon surface chemistry: changes upon impregnation with Al(III), Fe(III) and Zn(II)-metal oxide catalyst precursors from NO_3^- aqueous solutions. *Arabian Journal of Chemistry*, 12(8):3963-3976. https://doi.org/10.1016/j.arabjc.2016.02.018

Budania R, Dangayach S, 2023. A comprehensive review on permeable reactive barrier for the remediation of groundwater contamination. *Journal of Environmental Management*, 332:117343. https://doi.org/10.1016/j.jenvman.2023.117343

Chen FY, Yang Y, Chang M, et al., 2013. Release performance and mechanism of the slow-released persulfate materials. *Research of Environmental Sciences*, 26(9):995-1000 (in Chinese). https://doi.org/10.13198/j.issn.1001-6929.2013.09.013

CEN (Comité Européen de Normalisation), 2004. Leaching Characteristics of Moulded or Monolithic Building and Waste Materials. Determination of Leaching of Inorganic Components with the Diffusion Test. The Tank Test, EA NEN 7375. CEN.

Cheng S, Zhang LB, Xia HY, et al., 2016. Ultrasound and microwave-assisted preparation of Fe-activated carbon as an effective low-cost adsorbent for dyes wastewater treatment. *RSC Advances*, 6(82):78936-78946. https://doi.org/10.1039/c6ra14082c

Clifton CL, Huie RE, 1989. Rate constants for hydrogen abstraction reactions of the sulfate radical, $SO_4^{-}\cdot$ alcohols. *International Journal of Chemical Kinetics*, 21(8):677-687. https://doi.org/10.1002/kin.550210807

Das K, Kendall C, Isabelle M, et al., 2008. FTIR of touch imprint cytology: a novel tissue diagnostic technique. *Journal of Photochemistry and Photobiology B: Biology*, 92(3):160-164. https://doi.org/10.1016/j.jphotobiol.2008.05.012

Dong B, Zhang RZ, Gan YD, et al., 2019. Multiple methods for the identification of heavy metal sources in cropland soils from a resource-based region. *Science of The Total Environment*, 651:3127-3138. https://doi.org/10.1016/j.scitotenv.2018.10.130

Dong CD, Chen CW, Hung CM, 2019. Persulfate activation with rice husk-based magnetic biochar for degrading PAEs in marine sediments. *Environmental Science and Pollution Research*, 26(33):33781-33790. https://doi.org/10.1007/s11356-018-2423-2

Dumont G, Robert T, Marck N, et al., 2017. Assessment of multiple geophysical techniques for the characterization of municipal waste deposit sites. *Journal of Applied Geophysics*, 145:74-83. https://doi.org/10.1016/j.jappgeo.2017.07.013

Feng MB, Qu RJ, Zhang XL, et al., 2015. Degradation of flumequine in aqueous solution by persulfate activated with common methods and polyhydroquinone-coated magnetite/multiwalled carbon nanotubes catalysts. *Water Research*, 85:1-10. https://doi.org/10.1016/j.watres.2015.08.011

Gong YN, Li DL, Luo CZ, et al., 2017. Highly porous graphitic biomass carbon as advanced electrode materials for supercapacitors. *Green Chemistry*, 19(17):4132-4140. https://doi.org/10.1039/c7gc01681f

Goyal H, Tyagi T, Mondal P, 2023. Life cycle analysis and economic evaluation of adsorptive removal of arsenic from groundwater using GAC and GAC-Fe adsorbents. *Journal of Cleaner Production*, 429:139557. https://doi.org/10.1016/j.jclepro.2023.139557

Guo X, 2013. Advanced Treatment of Papermaking Wastewater by Sulfate Radical-Based Advanced Oxidation Process.

MS Thesis, South China University of Technology, Guangzhou, China (in Chinese).

Han ZY, Ma HN, Shi GZ, et al., 2016. A review of groundwater contamination near municipal solid waste landfill sites in China. *Science of The Total Environment*, 569-570: 1255-1264. https://doi.org/10.1016/j.scitotenv.2016.06.201

Hussain I, Li MY, Zhang YQ, et al., 2017. Insights into the mechanism of persulfate activation with nZVI/BC nanocomposite for the degradation of nonylphenol. *Chemical Engineering Journal*, 311:163-172. https://doi.org/10.1016/j.cej.2016.11.085

Kalaruban M, Loganathan P, Nguyen TV, et al., 2019. Iron-impregnated granular activated carbon for arsenic removal: application to practical column filters. *Journal of Environmental Management*, 239:235-243. https://doi.org/10.1016/j.jenvman.2019.03.053

Kamaraj M, Srinivasan NR, Assefa G, et al., 2020. Facile development of sunlit ZnO nanoparticles-activated carbon hybrid from pernicious weed as an operative nano-adsorbent for removal of methylene blue and chromium from aqueous solution: extended application in tannery industrial wastewater. *Environmental Technology & Innovation*, 17: 100540. https://doi.org/10.1016/j.eti.2019.100540

Kang N, Hua I, Rao PSC, 2004. Production and characterization of encapsulated potassium permanganate for sustained release as an in situ oxidant. *Industrial & Engineering Chemistry Research*, 43(17):5187-5193. https://doi.org/10.1021/ie0499097

Khursan SL, Semes'ko DG, Safiullin RL, 2006. Quantum-chemical modeling of the detachment of hydrogen atoms by the sulfate radical anion. *Russian Journal of Physical Chemistry*, 80(3):366-371. https://doi.org/10.1134/s0036024406030113

Kosson DS, van der Sloot HA, Eighmy TT, 1996. An approach for estimation of contaminant release during utilization and disposal of municipal waste combustion residues. *Journal of Hazardous Materials*, 47(1-3):43-75. https://doi.org/10.1016/0304-3894(95)00109-3

Krishnan KA, Haridas A, 2008. Removal of phosphate from aqueous solutions and sewage using natural and surface modified coir pith. *Journal of Hazardous Materials*, 152(2): 527-535. https://doi.org/10.1016/j.jhazmat.2007.07.015

Lee ES, Schwartz FW, 2007. Characteristics and applications of controlled-release $KMnO_4$ for groundwater remediation. *Chemosphere*, 66(11):2058-2066. https://doi.org/10.1016/j.chemosphere.2006.09.093

Lee ES, Gupta N, 2014. Development and characterization of colloidal silica-based slow-release permanganate gel (SRPG): laboratory investigations. *Chemosphere*, 109:195-201. https://doi.org/10.1016/j.chemosphere.2014.01.020

Lee YC, Li YF, Chen MJ, et al., 2020. Efficient decomposition of perfluorooctanic acid by persulfate with iron-modified activated carbon. *Water Research*, 174:115618. https://doi.org/10.1016/j.watres.2020.115618

Li HY, 2018. Investigation of Typical Organics for Activate Persulfate Degradation. MS Thesis, China University of Petroleum (Beijing), Beijing, China (in Chinese).

Li J, Yang ZH, Xu HY, et al., 2016. Electrochemical treatment of mature landfill leachate using Ti/RuO_2–IrO_2 and Al electrode: optimization and mechanism. *RSC Advances*, 6(53):47509-47519. https://doi.org/10.1039/c6ra05080h

Li Z, 2016. Cranular Activated Carbon Supported Iron as a Heterogeneous Persufate Catalyst for the Pretreatment of Mature Landfill Leachate. MS Thesis, Donghua University, Shanghai, China (in Chinese).

Li ZJ, Yang Q, Zhong Y, et al., 2016. Granular activated carbon supported iron as a heterogeneous persulfate catalyst for the pretreatment of mature landfill leachate. *RSC Advances*, 6(2):987-994. https://doi.org/10.1039/c5ra21781d

Liang SH, Kao CM, Kuo YC, et al., 2011. In situ oxidation of petroleum-hydrocarbon contaminated groundwater using passive ISCO system. *Water Research*, 45(8):2496-2506. https://doi.org/10.1016/j.watres.2011.02.005

Lin CW, Wu CH, Tang CT, et al., 2012. Novel oxygen-releasing immobilized cell beads for bioremediation of BTEX-contaminated water. *Bioresource Technology*, 124:45-51. https://doi.org/10.1016/j.biortech.2012.07.099

Ma HR, Zhang X, Feng GQ, et al., 2023a. Carbon nanotube membrane armed with confined iron for peroxymonosulfate activation towards efficient tetracycline removal. *Separation and Purification Technology*, 312:123319. https://doi.org/10.1016/j.seppur.2023.123319

Ma HR, Xu S, Zhang X, et al., 2023b. N-doped coal-based carbon membrane coupling peroxymonosulfate activation for bisphenol a degradation: the role of micro-carbon structure and nitrogen species. *Journal of Cleaner Production*, 423:138713. https://doi.org/10.1016/j.jclepro.2023.138713

Mehrabi N, Soleimani M, Yeganeh MM, et al., 2015. Parameter optimization for nitrate removal from water using activated carbon and composite of activated carbon and Fe_2O_3 nanoparticles. *RSC Advances*, 5(64):51470-51482. https://doi.org/10.1039/c5ra03920g

Neta P, Madhavan V, Zemel H, et al., 1977. Rate constants and mechanism of reaction of sulfate radical anion with aromatic compounds. *Journal of the American Chemical Society*, 99(1):163-164. https://doi.org/10.1021/ja00443a030

Omoike AI, Harmon D, 2019. Slow-releasing permanganate ions from permanganate core-manganese oxide shell particles for the oxidative degradation of an algae odorant in water. *Chemosphere*, 223:391-398. https://doi.org/10.1016/j.chemosphere.2019.02.036

Padmaja S, Alfassi ZB, Neta P, et al., 1993. Rate constants for reactions of SO_4^- radicals in acetonitrile. *International Journal of Chemical Kinetics*, 25(3):193-198. https://doi.org/10.1002/kin.550250307

Rauscher L, Sakulthaew C, Comfort S, 2012. Using slow-release permanganate candles to remediate PAH-contaminated water. *Journal of Hazardous Materials*, 241-242:441-449. https://doi.org/10.1016/j.jhazmat.2012.09.064

Ross C, Murdoch LC, Freedman DL, et al., 2005. Characteristics of potassium permanganate encapsulated in polymer. *Journal of Environmental Engineering*, 131(8):1203-1211. https://doi.org/10.1061/(ASCE)0733-9372(2005)131:8(1203)

Sakulthaew C, Chokejaroenrat C, 2016. Oxidation of 17β-estradiol in water by slow-release permanganate candles. *Environmental Engineering Science*, 33(4):224-234. https://doi.org/10.1089/ees.2015.0456

Singh R, Chakma S, Birke V, 2023. Performance of field-scale permeable reactive barriers: an overview on potentials and possible implications for in-situ groundwater remediation applications. *Science of the Total Environment*, 858:158838. https://doi.org/10.1016/j.scitotenv.2022.158838

Song XL, Wang C, Liu MQ, et al., 2018. Advanced treatment of biologically treated coking wastewater by persulfate oxidation with magnetic activated carbon composite as a catalyst. *Water Science and Technology*, 77(7):1891-1898. https://doi.org/10.2166/wst.2018.069

Tian WJ, Zhang HY, Qian Z, et al., 2018. Bread-making synthesis of hierarchically Co@C nanoarchitecture in heteroatom doped porous carbons for oxidative degradation of emerging contaminants. *Applied Catalysis B: Environmental*, 225:76-83. https://doi.org/10.1016/j.apcatb.2017.11.056

Tsitonaki A, Petri B, Crimi M, et al., 2010. In situ chemical oxidation of contaminated soil and groundwater using persulfate: a review. *Critical Reviews in Environmental Science and Technology*, 40(1):55-91. https://doi.org/10.1080/10643380802039303

Veerakumar P, Muthuselvam IP, Hung CT, et al., 2016. Biomass-derived activated carbon supported Fe_3O_4 nanoparticles as recyclable catalysts for reduction of nitroarenes. *ACS Sustainable Chemistry & Engineering*, 4(12):6772-6782. https://doi.org/10.1021/acssuschemeng.6b01727

Wang B, Zhang YZ, Gao CY, et al., 2023. Developing novel persulfate pellets to remediate BTEXs-contaminated groundwater. *Journal of Water Process Engineering*, 52:103505. https://doi.org/10.1016/j.jwpe.2023.103505

Wang J, 2017. Study on Treatment of Refractory Organic Wastewater by Persulfate Activated by Iron Based Sludge-Derived Biochar. PhD Thesis, Huazhong University of Science and Technology, Wuhan, China (in Chinese).

Wang Z, Lu YS, Wu ZL, et al., 2014. Study on the interference of persulfate in the process of COD determination and its elimination. *Industrial Water Treatment*, 34(8):78-81 (in Chinese). https://doi.org/10.11894/1005-829x.2014.34(8).078

Xu XY, Zeng GM, Peng YR, et al., 2012. Potassium persulfate promoted catalytic wet oxidation of fulvic acid as a model organic compound in landfill leachate with activated carbon. *Chemical Engineering Journal*, 200-202:25-31. https://doi.org/10.1016/j.cej.2012.06.029

Yang J, 2016. Study on Advanced Treatment of Landfill Leachate by Persulfate. MS Thesis, China University of Geosciences (Beijing), Beijing, China (in Chinese).

Yang S, Oostrom M, Truex MJ, et al., 2016. Injectable silica-permanganate gel as a slow-release MnO_4^- source for groundwater remediation: rheological properties and release dynamics. *Environmental Science: Processes & Impacts*, 18(2):256-264. https://doi.org/10.1039/c5em00559k

Yao YJ, Chen H, Qin JC, et al., 2016. Iron encapsulated in boron and nitrogen codoped carbon nanotubes as synergistic catalysts for fenton-like reaction. *Water Research*, 101:281-291. https://doi.org/10.1016/j.watres.2016.05.065

Ye JS, Chen X, Chen C, et al., 2019. Emerging sustainable technologies for remediation of soils and groundwater in a municipal solid waste landfill site–a review. *Chemosphere*, 227:681-702. https://doi.org/10.1016/j.chemosphere.2019.04.053

Zeng XL, Huang YZ, Zhang Y, et al., 2017. Elimination of persulfate interference in determination of COD in organic wastewater. *Journal of Chongqing University*, 40(12):79-86 (in Chinese). https://doi.org/10.11835/j.issn.1000-582X.2017.12.010

Zhang L, Tu LY, Liang Y, et al., 2018. Coconut-based activated carbon fibers for efficient adsorption of various organic dyes. *RSC Advances*, 8(74):42280-42291. https://doi.org/10.1039/c8ra08990f

Zhang XL, Feng MB, Qu RJ, et al., 2016. Catalytic degradation of diethyl phthalate in aqueous solution by persulfate activated with nano-scaled magnetic $CuFe_2O_4$/MWCNTs. *Chemical Engineering Journal*, 301:1-11. https://doi.org/10.1016/j.cej.2016.04.096

Zhao JJ, Sun YJ, Zhang Y, et al., 2021. Heterogeneous activation of persulfate by activated carbon supported iron for efficient amoxicillin degradation. *Environmental Technology & Innovation*, 21:101259. https://doi.org/10.1016/j.eti.2020.101259

Zhao JJ, Sun YJ, Zhang BT, et al., 2023. Amoxicillin degradation in the heat, light, or heterogeneous catalyst activated persulfate systems: comparison of kinetics, mechanisms and toxicities. *Journal of Environmental Management*, 348:119386. https://doi.org/10.1016/j.jenvman.2023.119386